PCCP

RSC Publishing

PAPER

Study on UV-shielding mechanism of layered double hydroxide materials†

Cite this: *Phys. Chem. Chem. Phys.*, 2013, **15**, 18217

Wenying Shi, Yanjun Lin, Shitong Zhang, Rui Tian, Ruizheng Liang, Min Wei,* David G. Evans and Xue Duan

Received 5th July 2013,
Accepted 8th August 2013

DOI: 10.1039/c3cp52819g

www.rsc.org/pccp

The development of UV-shielding materials has attracted considerable attention in the field of coatings and sunscreen. This paper reports the UV-shielding mechanism of layered double hydroxide (LDH) materials in terms of chemical composition, structure and morphology, by using $(LDH/PAA)_n$ films (n stands for bilayer number) through alternate LBL assembly of LDH nanoparticles and poly(acrylic acid) (PAA) on quartz substrates as a model system. A combination investigation based on experimental and theoretical study demonstrates that the maximum UV scattering can be achieved when $\lambda/d \approx 1.98$; the introduction of Zn element is an effective way to tune the electron structure, band gap, transition mode and resulting UV-shielding property of LDH materials. A UV-shielding efficiency as high as 95% can be obtained by modulating the particle size, composition and thickness of the LDHs. Furthermore, the UV anti-aging capacity of LDH-modified bitumen was studied, which demonstrates a large improvement in UV-resistance performance of bitumen by the incorporation of LDH materials. Therefore, this work systematically discloses the relationship between UV-shielding property and chemical/structural parameters of LDH materials, which can be potentially used as anti-aging agents in various organic matrices and polymer areas.

1. Introduction

The solar spectrum is a complex band of radiation including UVC (220–290 nm), UVB (290–320 nm), UVA (320–400 nm) as well as visible and infrared light. The UV-light with short wavelength and high energy can destroy the covalent bonds (*e.g.*, C–H, C–C, C–Cl) of organic substances, which results in serious damage to commonly used organic materials, as well as human health.[1] Therefore, the development of UV-shielding materials has attracted considerable attention in the field of coatings and sunscreen, so as to reduce the destruction of UV irradiation. Generally, inorganic UV-shielding materials (*e.g.*, TiO_2, ZnO, SiO_2, and Al_2O_3) have been widely used, owing to their optical and thermal stability as well as nontoxicity. However, their photocatalytic activity as a side-effect would induce photo-degradation of organic substances simultaneously.[2] Therefore, it is necessary to search for novel UV-shielding materials with high stability and excellent light shielding behavior.

Layered double hydroxides (LDHs), whose structure can be generally expressed as $[M^{II}_{1-x}M^{III}_{x}(OH)_2](A^{n-})_{x/n}\cdot mH_2O$ (M^{II} and M^{III} are divalent and trivalent metals respectively; A^{n-} a n-valent anion), are one type of important inorganic layered material which represent a large versatility in terms of their chemical composition and their ability to build up 2D-organized structures.[3] They are available as both naturally occurring minerals and synthetic materials, which have been widely explored in the fields of catalysis, separation, biology, drugs and functional additives.[4] LDH-based UV-shielding materials have been reported, which show significantly enhanced performance compared with organic UV absorbents.[5] However, a key problem remains unresolved for the UV-shielding mechanism of LDH materials, which greatly limits the understanding of structure–property correlation as well as the design/fabrication of superior functional materials. Therefore, it is highly essential to systematically study the relationship between UV-shielding behavior and chemical/structural parameters, so as to achieve a new type of LDH-based materials with largely enhanced UV-shielding performance.

Herein, the UV-shielding mechanism of LDH materials and their predominant influential factors were investigated in detail, by using $(LDH/PAA)_n$ films (n stands for bilayer number) through alternate LBL assembly of LDH nanoparticles and poly(acrylic acid) (PAA) on quartz substrates as a model system. A combination investigation based on experimental and theoretical study demonstrates that the physical morphology, chemical

State Key Laboratory of Chemical Resource Engineering, Beijing University of Chemical Technology, Beijing 100029, China. E-mail: weimin@mail.buct.edu.cn; Fax: +86-10-64425385; Tel: +86-10-64412131

† Electronic supplementary information (ESI) available: Side view of SEM images (Fig. S1), particle size distributions (Fig. S2), TEM images (Fig. S3) and photoluminescence spectra (Fig. S4) and the light intensity decay data (Table S1). See DOI: 10.1039/c3cp52819g

composition and multilayer architecture of LDH particles impose great influence on the scattering and absorption of UV-light. A UV-shielding efficiency as high as 95% can be obtained by tuning the particle size, composition and thickness of the LDHs. In addition, the UV-shielding property of LDH materials was studied in a base bitumen system, and it was found that both the stability and service lifetime of bitumen increase significantly, demonstrating a large improvement in the UV-resistance capability of bitumen by the incorporation of LDH materials.

2. Experimental

2.1 Materials

Analytical grade chemicals including $Zn(NO_3)_2$, $Al(NO_3)_3$, NaOH, H_2SO_4, NH_3, H_2O_2, $Mg(NO_3)_2$, PAA and UV 531 were used without further purification. SiO_2 and TiO_2 nanoparticles (nano-SiO_2, nano-TiO_2) were purchased from Sigma-Aldrich Co. Deionized and decarbonated water wasused in all the experimental processes. Bitumen (AH-90 paving bitumen) was obtained from the Panjin Petrolium Asphalt Factory in the Gansu Province of China.

2.2 Preparation of the LDH nanoparticles and the $(LDH/PAA)_n$ films

The Mg_2Al–CO_3–LDHs (t stands for the crystallization time: t = 2, 8, 12, 24, 36, 48, 56, 150 and 220 h, respectively) and $(Zn_xMg_y)_2Al$–CO_3–LDHs with different Zn^{2+}/Mg^{2+} ratios ($x:y$ = 1 : 4, 2 : 3, 1 : 1, 3 : 2, 4 : 1, 1 : 0; $x + y = 1.0$) were synthesized by the hydrothermal method reported previously.[6] For the fabrication of the $(LDH/PAA)_n$ films, the quartz glass substrate was cleaned in concentrated NH_3/30% H_2O_2 (7 : 3, v/v) and concentrated H_2SO_4 for 30 min each. After each procedure, the quartz substrate was rinsed and washed thoroughly with deionized water. The substrate was dipped in a colloidal suspension (0.1 g mL^{-1}) of the LDH nanoparticles for 10 min followed by washing thoroughly, and then was immersed into 100 mL of PAA aqueous solution (0.025 wt%) for another 10 min followed by washing. Multilayer films of $(LDH/PAA)_n$ were fabricated by alternate deposition of the LDH nanopaticles and PAA for n cycles. The resulting films were dried with a nitrogen gas flow for 2 min at 25 °C.

2.3 Preparation of the LDH-modified bitumen

The LDH-modified bitumen was prepared using a high shear mixer. Bitumen was first heated until it becomes awell fluid at ~140 °C in the mixer. Subsequently, UV 531, nano-SiO_2, nano-TiO_2 and Mg_2Al–CO_3–LDH was added into bitumen with 5% (w), respectively, and the mixture was blended at 4000 rpm for 1 h.

2.4 UV-aging test procedure

The UV-aging test was performed in a chamber with UV lamp of 500 W and the intensity of 15 000 μW cm^{-2}. The melted bitumen was placed on a iron pan located in the bottom of the chamber at 50 °C for 12 days. The thickness of the bitumen film was ~1.25 mm.

2.5 Characterization techniques

The UV-vis absorption spectra were collected in the range from 200 to 800 nm on a Shimadzu T-9201 spectrophotometer, with the slit width of 1.0 nm. The fluorescence spectra were performed on a RF-5301PC fluorospectrophotometer with the excitation wavelength of 325 nm. The fluorescence emission spectra ranged from 300–560 nm, and both the excitation and emission slits were set to 3 nm. X-ray diffraction patterns (XRD) were recorded using a Rigaku 2500 VB2+PC diffractometer under the conditions: 40 kV, 50 mA, Cu Kα radiation (λ = 0.154 nm) step-scanned with a scanning rate of 0.5° min^{-1}, and a 2θ angle ranging from 2 to 70°. The morphology of films was investigated by using a scanning electron microscope (SEM, ZEISS) and transmission electron microscope (TEM, JEOL JEM-2100), and the accelerating voltages applied were 20 kV and 200 kV, respectively. The surface roughness data were obtained by using the atomic force microscopy (AFM) software (Digital Instruments, version 6.12). The softening point was tested according to ASTM D36. A Brookfield viscometer (Model DV-II+, Brookfield Engineering Inc., USA) was employed to measure the viscosity of the bitumen according to ASTM D4402.

2.6 Calculation details

The geometries of the cluster models were fully optimized with the density functional theory (DFT) method of B3LYP.[7] Anions and water molecules are intercalated at random positions. UV-vis optical absorption calculations of LDH models were performed in the framework of the spin-polarized density functional perturbation theory (PT) implemented in VASP 5.2[8] by employing the HSE0650 exchange–correlation function. The optical properties were calculated through the frequency-dependent dielectric function $\varepsilon(\omega) = \varepsilon_1(\omega) + i\varepsilon_2(\omega)$ following a methodology.[9] Pre- and post-processing operations of optical response were performed with the graphical interface MedeA.[10]

3. Results and discussion

3.1 Structural and morphological characterization

Fig. 1 shows the powder XRD patterns of Mg_2Al–CO_3–LDHs (t = 2, 8, 12, 24, 36, 48, 56, 150 and 220 h, respectively) and $(Zn_xMg_y)_2Al$–CO_3–LDHs ($x:y$ = 1 : 4, 2 : 3, 1 : 1, 3 : 2, 4 : 1 and 1 : 0; $x + y = 1.0$). All the patterns of these samples can be indexed to a hexagonal lattice. The two sharp and intense characteristic diffraction peaks appearing as symmetric lines at 2θ 11° and 22° are ascribed to the (003) and (006) planes. The basal spacing (d_{003} = ~1.18 nm) is consistent with the presence of carbonate as charge compensating anions in the interlayer space. For the Mg_2Al–CO_3–LDH (t), the increase in intensity and decrease in half-peak-width of (003) and (006) reflection upon prolonging the crystallization time indicate the enhancement of crystallinity. In the case of $(Zn_xMg_y)_2Al$–CO_3–LDHs, both the intensity and half-peak-width show no significant change with various Zn^{2+}/Mg^{2+} ratios, demonstrating chemical composition imposes no obvious effect on the crystallinity of LDHs.

In order to investigate the UV-shielding behavior of LDH materials, the $(LDH/PAA)_n$ films were fabricated through

 This journal is © the Owner Societies 2013

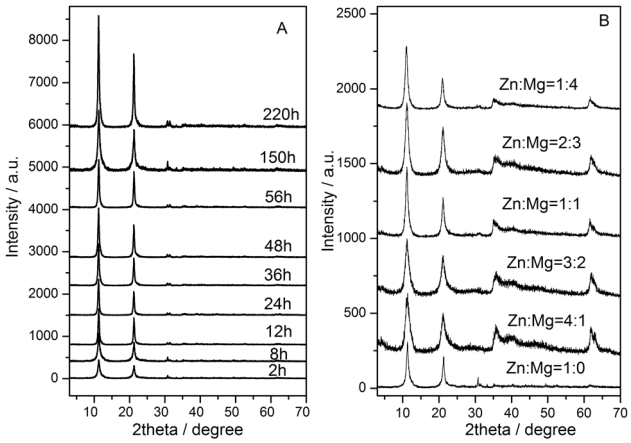

Fig. 1 (A) XRD patterns of powdered samples of (A) Mg_2Al–CO_3–LDHs (t = 2, 8, 12, 24, 36, 48, 56, 150 and 220 h, respectively); (B) $(Zn_xMg_y)_2Al$–CO_3–LDHs (x : y = 1 : 4, 2 : 3, 1 : 1, 3 : 2, 4 : 1 and 1 : 0; $x + y$ = 1.0).

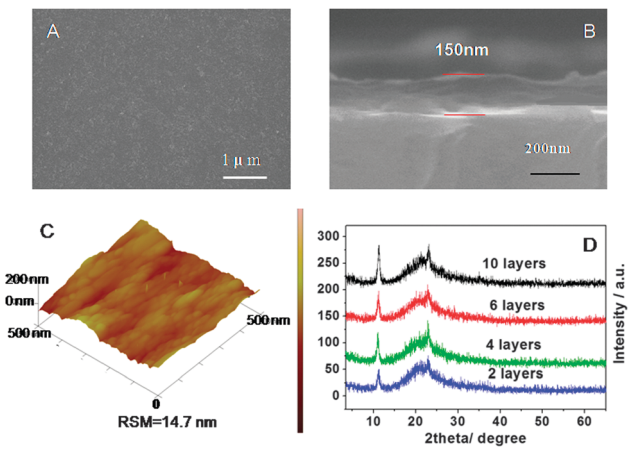

Fig. 2 (A–C) Top view, side view of SEM image and tapping-mode AFM image for the $(Mg_2Al$–CO_3–LDH/PAA$)_{10}$ film; (D) XRD pattern of the $(Mg_2Al$–CO_3–LDH/PAA$)_n$ films with n = 2, 4, 6 and 10, respectively.

alternate deposition of the LDH nanoparticles and PAA on quartz substrates as a model system. A typical top view of the SEM image for the $(Mg_2Al$–CO_3–LDH/PAA$)_{10}$ (t = 12 h) film shows that the surface is microscopically continuous and smooth (Fig. 2A), with a film thickness of 150 nm observed from its side view SEM image (Fig. 2B). The approximately linear increase of film thickness as a function of bilayer number confirms a uniform and periodic layered structure (Fig. S1, ESI†), from which the thickness of one bilayer $(Mg_2Al$–CO_3–LDH/PAA$)_1$ was estimated to be ~15 nm. The AFM topographical image (Fig. 2C) shows the morphology and roughness information of the film, with a root-mean square roughness of 14.7 nm. XRD patterns (Fig. 2D) exhibit a Bragg peak at 2θ 11.8° and its intensity increases successively upon increasing n, which can be attributed to a superlattice structure in the normal direction of the film.

3.2 UV-shielding mechanism of LDH materials

In order to clarify the UV-shielding mechanism, the structure–property relationship of LDH materials is discussed from the viewpoint of physical morphology and chemical composition of LDHs, respectively.

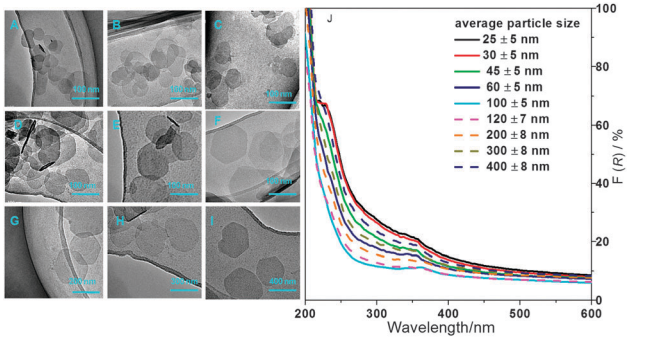

Fig. 3 (A–I) TEM images of the Mg_2Al–CO_3–LDH (t = 2, 8, 12, 24, 36, 48, 56, 150 and 220 h, respectively) nanoparticles; (J) diffusion reflection spectra of the $(Mg_2Al$–CO_3–LDH/PAA$)_{10}$ films with various particle size. The average particle size of LDH was determined according to the equation $d = \Sigma n_i d_i / n_i$ by randomly measuring ~100 particles by TEM. The standard deviation was calculated from the formula $\sigma = [(\Sigma(d_i - d)^2)/\Sigma n_i]^{1/2}$.

The effect of physical morphology on the UV scattering capacity. TEM images (Fig. 3A–I) and particle size distribution (Fig. S2, ESI†) of the Mg_2Al–CO_3–LDH (t = 2, 8, 12, 24, 36, 48, 56, 150 and 220 h, respectively) nanoparticles show the particle diameter increases in the range 25–400 nm, demonstrating the enhancement in particle size with prolonging crystallization time. Fig. 3J displays the UV-vis diffuse reflection spectra of $(Mg_2Al$–CO_3–LDH/PAA$)_{10}$ (t = 2, 8, 12, 24, 36, 48, 56, 150 and 220 h, respectively) films, in which a lower diffuse reflection absorption coefficient $F(R)$ indicates a higher scattering property according to Munk–Kubelka theory.[11] It is observed that the $F(R)$ decreases remarkably with the increase of particle size (from 25 to 100 nm) firstly, and then turns to an obvious increment with further increase of particle size (from 200 to 400 nm). The optimum particle size of LDHs for light scattering is 100–200 nm due to the lowest $F(R)$. In addition, the optimum particle size of LDHs for light scattering can also be predicted by the light-scattering theory:[12]

$$S = \frac{\alpha M^3 \lambda^{\frac{1}{2}}}{\frac{\lambda^2}{2d} + n_b^2 \pi^2 M d} \quad (1)$$

$$M = 0.4(n_p - n_b) \quad (2)$$

where S is the scattering coefficient; α is a constant (related to the material property); λ is the wavelength of incident light; n_p and n_b are the refractive index of the dispersed phase and the dispersed medium, respectively; d is the diameter of particles. For this system, n_p is 1.5 and n_b is 1.0. For a certain wavelength of incident light, the maximum S value can be obtained when $\lambda/d = n_b\pi(2M)^{1/2} \approx 1.98$. Consequently, the diameter of LDH particles for maximum scattering of UV-light (200–400 nm) was calculated in the range 101–202 nm, which approximates the experimental results.

The effect of chemical composition on the UV absorption capacity. In an effort to study the effect of chemical composition of LDHs on the UV absorption capacity, Zn element is

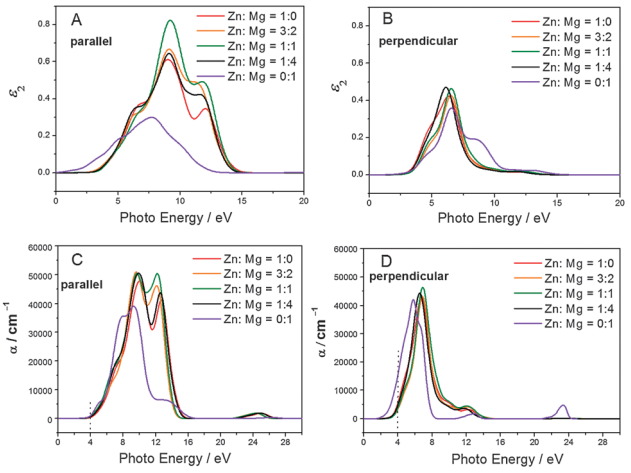

Fig. 4 (A,B) The imaginary part ε_2 of the dielectric function (ε) and (C,D) absorption coefficient (α) spectra of the $(Zn_xMg_y)_2Al–CO_3$–LDHs with various Zn^{2+}/Mg^{2+} ratios under parallel and perpendicular polarization, respectively.

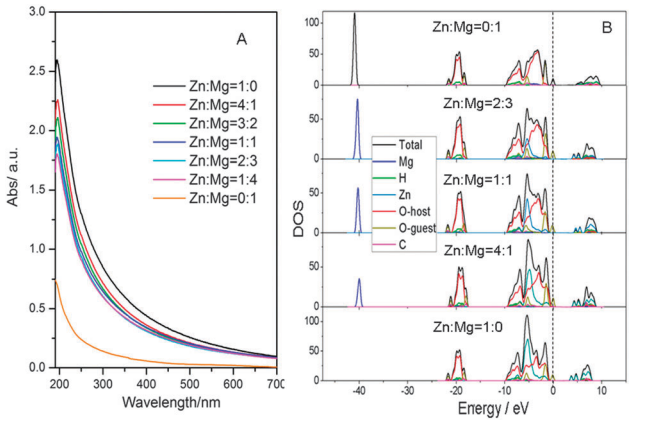

Fig. 5 (A) UV-vis absorption spectra of the $((Zn_xMg_y)_2Al–CO_3–LDH/PAA)_{10}$ films ($x:y = 1:0, 4:1, 3:2, 1:1, 2:3, 1:4$ and $0:1$; $x + y = 1.0$); (B) the density of states for the $(Zn_xMg_y)_2Al–CO_3$–LDHs ($x:y = 0:1, 2:3, 1:1, 4:1$ and $1:0$; $x + y = 1.0$).

introduced into the crystal lattice of the $Mg_2Al–CO_3$–LDHs. The optical properties of LDHs are studied using the dielectric function and absorption coefficient. The dielectric function $\varepsilon(\omega)$ with the real part $\varepsilon_1(\omega)$ and imaginary part $\varepsilon_2(\omega)$ is usually used to describe the linear optical properties of the system. In particular, the $\varepsilon_2(\omega)$ represents real transitions between occupied and unoccupied electronic states.[13] The $\varepsilon_2^{\parallel}(\omega)$ and $\varepsilon_2^{\perp}(\omega)$ under parallel and perpendicular polarization light are calculated and shown in Fig. 4. For parallel polarization, the $Mg_2Al–CO_3$–LDH shows no obvious peak, indicating the absence of the transition among Mg, Al and O (Fig. 4A). However, the $(Zn_xMg_y)_2Al–CO_3$–LDHs ($x:y$ = 3:2, 1:1, 1:4 and 1:0; $x + y = 1.0$) reveal three peaks originating from the electron transitions between O 2p and Zn 4s (6.50 eV), Zn 3d and O 2p (9.21 eV) as well as Zn 3d and O 2s (12.1 eV), respectively. The $\varepsilon_2^{\parallel}(\omega)$ at 9.21 and 12.1 eV increases at first to a maximum and then decreases with the increase of the Zn^{2+}/Mg^{2+} ratio. The maximum $\varepsilon_2^{\parallel}$ presents in the sample when $Zn^{2+}/Mg^{2+} = 1$, verifying the synergistic effects of Mg and Zn. In the case of perpendicular polarization, the $\varepsilon_2^{\perp}(\omega)$ spectra of the $(Zn_xMg_y)_2Al–CO_3$–LDHs show three peaks (4.5, 6.5 and 12.0 eV), corresponding to the electron transitions between the O and Zn atom. The decreased intensity and redshift of $\varepsilon_2^{\perp}(\omega)$ spectra compared with those of $\varepsilon_2^{\parallel}(\omega)$ demonstrate a moderate optical anisotropy with respect to light polarization (Fig. 4B). The electric field perpendicular to the axis is in general strongly screened,[14] which is known as the depolarization effect. It would substantially reduce the magnitude of the $\varepsilon_2(\omega)$ spectrum for the perpendicular light polarization, and therefore enhance the optical anisotropy.

The absorption coefficient α, which stands for the decay of light intensity spreading in unit distance, was calculated. Fig. 4C and D display α for light polarized parallel ($E\|c$) and perpendicular ($E\perp c$) to the c axis of the LDH microcrystal, respectively. The different absorption edges ($E\perp c$ is situated at lower energy than $E\|c$) and peak shape indicate a significant optical anisotropy. Compared with the $Mg_2Al–CO_3$–LDHs (5.01, 7.70, 9.41 and 13.3 eV), the absorption edges for the $(Zn_xMg_y)_2Al–CO_3$–LDHs (7.02, 10.1 and 12.0 eV) show a blue-shift accompanied with intensity enhancement, indicating that the Zn element is beneficial to the increase in UV absorption capacity. The maximum absorption coefficient in the sample with Zn^{2+}/Mg^{2+} = 1 agrees well with the dielectric function results, further demonstrating the synergistic effects of Mg and Zn.

Fig. 5A shows the absorption spectra of the $((Zn_xMg_y)_2Al–CO_3–LDH/PAA)_{10}$ films with the same particle size (100 nm, Fig. S3, ESI†) but different Zn^{2+}/Mg^{2+} ratios. The results show that the UV absorption intensity enhances along with the increase of the Zn^{2+}/Mg^{2+} ratio, indicating the Zn element facilitates the absorption of photons and the resulting electron transition. In addition, the photoluminescence intensity of the $((Zn_xMg_y)_2Al–CO_3–LDH/PAA)_{10}$ films at 350–375 nm increases with the increase of Zn^{2+}/Mg^{2+} ratio (Fig. S4, ESI†), which suggests the enhancement of electron–hole recombination.

To obtain the electronic structure information for the effect of the Zn element on the UV absorption capacity, the density of states (DOS) of the $(Zn_xMg_y)_2Al–CO_3$–LDHs are calculated and shown in Fig. 5B. For $Mg_2Al–CO_3$–LDH, Mg 2p, O 2s and O 2p state of host layers dominate from −42.0 to −40.0 eV, from −21.0 to −17.0 eV and from −10.0 to 0.0 eV, respectively. The absence in energy level transition between the Mg and Al atoms indicates the UV absorption of the $Mg_2Al–CO_3$–LDHs is mainly contributed from the interlayer CO_3^{2-} anions. In contrast, the $(Zn_xMg_y)_2Al–CO_3$–LDH samples possess two new peaks originating from Zn 3d (from −10.0 to 0.0 eV) and Zn 4s (from 2.0 to 7.0 eV). The peak intensity rises gradually with the increase of Zn^{2+}/Mg^{2+} ratio, implying the enhancement of UV absorption capacity. Furthermore, compared with the $Mg_2Al–CO_3$–LDHs (4.58 eV), the decrease in band gap (3.33–4.16 eV) of the $(Zn_xMg_y)_2Al–CO_3$–LDHs testifies the increase in photon absorption efficiency. The maximum band gap (4.16 eV) presents in the sample of ZnMgAl–CO_3–LDH, further confirming the synergistic effects between Mg and Zn towards electron transition. Therefore, both the experimental and theoretical results show that the

 This journal is © the Owner Societies 2013

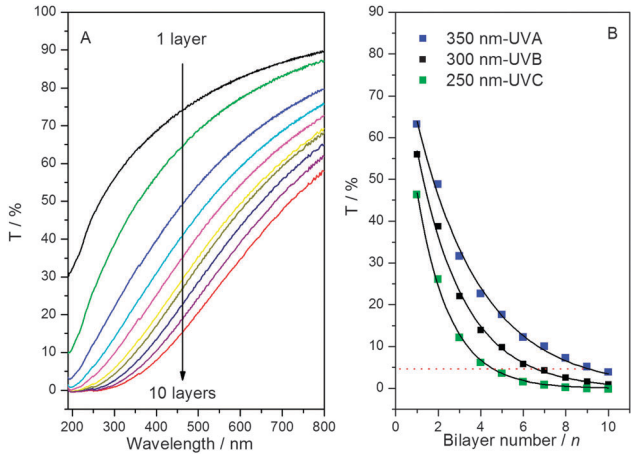

Fig. 6 (A) UV-vis transmission spectra of the $(ZnMgAl–CO_3–LDHs/PAA)_n$ (n = 1–10) films; (B) the transmittance of the films as a function of bilayer number.

introduction of Zn is an effective way to tune the electronic structure, band gap, transition mode and UV-shielding property.

The effect of multilayers on the UV-shielding capacity. The UV-vis transmission spectra of the $(ZnMgAl–CO_3–LDH/PAA)_n$ films with various bilayer numbers (n) were recorded and shown in Fig. 6A. It was observed that the transmittance of these films in 200–800 nm decreases along with the increase of n, indicating enhanced light shielding capacity. Fig. 6B shows the transmittance change at a specific wavelength as a function of bilayer number. The Lambert model (eqn (3))[15] was used to fit the experimental data. Taking into account both the reflections of incident and transmission plane, the Lambert model is modified (eqn (4)):

$$T = \frac{I}{I_0} = \exp(-\beta x) \tag{3}$$

$$T = \frac{I}{I_0} = (1 - R)^2 \exp(-\beta x) \tag{4}$$

where T, I, I_0, R, β and x are transmittance, transmitted intensity, incident intensity, reflection coefficient, absorption coefficient and film thickness, respectively.

The model parameters and the goodness of fit are reported in Table S1 (ESI†), from which the experimental T values agree well with the calculated ones obtained from the modified Lambert model with high regress coefficients ($r^2 > 0.996$). This indicates that the light decay of LDH with various film thickness accords with the one-exponential attenuation, which can be described by the modified Lambert model. The 95% UV light at 250 (UVC), 300 (UVB) and 350 nm (UVA) can be shielded by the LDH film with a thickness of 60 nm (4 layers), 105 nm (7 layers) and 135 nm (9 layers), respectively. This indicates that LDH materials show more significant shielding capacity towards high energy UVC.

3.3 UV resistance performance of LDH-modified bitumen

Bitumen consists of hydrocarbon mixtures with different molecular weights containing hetero atoms (S, N and O) as well as trace of metals (V and Ni), which is widely used in the fields of sealants, binders, waterproof coatings and paving materials.[16] However, the UV-aging of bitumen is a rather serious problem in practical applications, which leads to distinct shortening of the service life as well as the emission of large amount of VOCs.[17] The bitumen aging originates from the C–C bond cleavage of organic species and loss of volatile components caused by UV irradiation.[18] In order to evaluate the UV-shielding performance of LDH materials from the viewpoint of practical applications, the UV anti-aging capacity of LDH-modified bitumen was studied. Generally, the UV-aging of bitumen is evaluated in terms of the viscosity aging index (VAI) and softening point increment (ΔS), for both of which a less value indicates a higher UV resistance.[19] The two parameters can be expressed by the following formula:

Table 1 The evaluation parameters of the LDH-modified bitumen

	Mass percentage of LDH			
Parameter	0%	1%	3%	5%
Unaged viscosity/Pa s, 135 °C	0.33	0.38	0.48	0.49
Aged viscosity/Pa s, 135 °C, 4 d	14.1	4.20	2.40	2.10
VAI/%	41.7	9.90	4.00	3.30
Unaged softening point/°C	46.3	46.8	47.0	47.1
Aged softening point/°C, 4 d	84.2	83.4	79.9	79.0
ΔS/°C	37.9	36.6	32.9	31.9

$$\text{VAI} = \frac{\text{Aged viscosity value} - \text{Unaged viscosity value}}{\text{Unaged viscosity value}} \times 100\% \tag{5}$$

$$\Delta S = \text{Aged softening point value} - \text{Unaged softening point value} \tag{6}$$

The viscosity and softening point of LDH-modified bitumen under different conditions are shown in Table 1. It can be observed that both VAI and ΔS decrease along with the increase of mass percentage of LDH (w) from 0 to 5%, and the minimum values of VAI (3.3%) and ΔS (31.9 °C) were obtained with w = 5%. This mass percentage was therefore chosen in the following study. The commercial UV 531, SiO_2 and TiO_2 nanoparticles were used to modify base bitumen as comparison samples. Fig. 7 shows the VAI and ΔS values of base bitumen and the four modified bitumen after UV-aging for 12 days (the aging conditions in the laboratory are shown in Section 2.4). The results show that the VAI and ΔS values of all the four modified bitumen are lower than those of base bitumen. The LDH-modified bitumen displays the best anti-UV aging behavior: the VAI and ΔS values decrease by 70% (from 12.0% to 3.6%) and 64% (from 100 °C to 36 °C), respectively, much superior to those of comparison samples. The results demonstrate that LDH materials can be potentially used as a promising anti-aging agents, so as to enhance light stability and prolong service lifetime of bitumen and related materials.

4. Conclusions

In summary, the UV-shielding mechanism of LDH materials was systematically studied in terms of chemical/structural

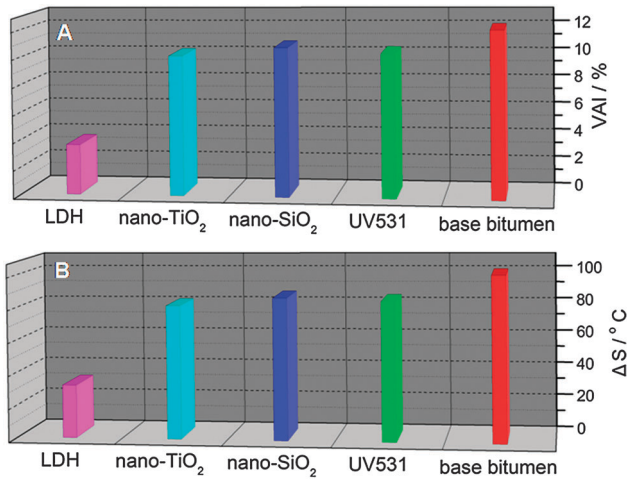

Fig. 7 The viscosity aging index and softening point increment of base bitumen and the four modified bitumen after irradiation with a UV lamp (500 W, 15 000 μW cm^{-2}) for 12 days in a laboratory.

parameters, by using the $(LDH/PAA)_n$ (n stands for bilayer numbers) films as a model system. The 95% UV light can be shielded by the LDH film *via* tuning the particle size, chemical composition and film thickness. The maximum UV scattering can be achieved when $\lambda/d \approx 1.98$. Both the experimental and theoretical results show that the introduction of Zn element is an effective way to tune the electron structure, band gap, transition mode and resulting UV-shielding properties. In addition, the practical application of UV-shielding performance of LDH materials was demonstrated in a bitumen system. Compared with the base bitumen, the VAI and ΔS of LDH-modified bitumen decrease by 70% and 64%, respectively, indicating a significant enhancement in the light stability of bitumen. Therefore, this work provides a detailed understanding on the correlation between structure and the UV-shielding property of LDHs materials, which can be potentially used as the anti-aging agent in bitumen and polymer materials.

Acknowledgements

This work was supported by the 973 (Grant No. 2014CB932104), the National Natural Science Foundation of China, the Fundamental Research Funds for the Central Universities.

Notes and references

1 M. Nowick, A. Richter, B. Wolf and H. Kaczmarek, *Polymer*, 2003, **44**, 6599.

2 (*a*) J. C. Yu, J. Yu, W. Ho, Z. Jiang and L. Zhang, *Chem. Mater.*, 2002, **14**, 3808; (*b*) R. Hong, T. Pan, J. Qian and H. Li, *Chem. Eng. J.*, 2006, **119**, 71; (*c*) L. Sronek, J. Majimel, Y. Kihn, Y. Montardi, A. Tressaud, M. Feist, C. Legein, J. Y. Buzare, M. Body and A. Demourgues, *Chem. Mater.*, 2007, **19**, 5111; (*d*) P. J. Nair, E. Wachtel, I. Lubomirsky, J. Fleig and J. Maier, *Adv. Mater.*, 2003, **15**, 2077.

3 (*a*) Q. Wang and D. O'Hare, *Chem. Rev.*, 2012, **112**, 4124; (*b*) J. Bauer, P. Behrens, M. Speckbacher and H. Langhals, *Adv. Funct. Mater.*, 2003, **13**, 241; (*c*) F. Millange, R. I. Walton, L. Lei and D. O'Hare, *Chem. Mater.*, 2000, **12**, 1990; (*d*) A. M. Fogg, G. R. Williams, R. Chester and D. O'Hare, *J. Mater. Chem.*, 2004, **14**, 2369.

4 (*a*) A. M. Fogg, V. M. Green, H. G. Harvey and D. O'Hare, *Adv. Mater.*, 1999, **11**, 1466; (*b*) J. H. Choy, S. Y. Kwak, J. S. Park, Y. J. Jeong and J. Portier, *J. Am. Chem. Soc.*, 1999, **121**, 1399; (*c*) D. Yan, J. Lu, M. Wei, S. Li, D. G. Evans and X. Duan, *Phys. Chem. Chem. Phys.*, 2012, **14**, 8591; (*d*) S. Fleutot, J. Dupin, G. Renaudin and H. Martinez, *Phys. Chem. Chem. Phys.*, 2011, **13**, 17564; (*e*) Y. Zhang, B. Cui, C. Zhao, H. Lin and J. Li, *Phys. Chem. Chem. Phys.*, 2013, **15**, 7363.

5 (*a*) W. Sun, Q. He, L. Lu and H. Liu, *Mater. Chem. Phys.*, 2008, **107**, 261; (*b*) S. B. Khan, C. Z. Liu, E. S. Jang, K. Akhtar and H. Han, *Mater. Lett.*, 2011, **65**, 2923; (*c*) G. J. Cui, X. Y. Xu, Y. J. Lin, D. G. Evans and D. Q. Li, *Ind. Eng. Chem. Res.*, 2010, **49**, 448; (*d*) H. Chai, Y. J. Lin, D. G. Evans and D. Q. Li, *Ind. Eng. Chem. Res.*, 2008, **47**, 2855.

6 Z. P. Xu, G. Stevenson, C. Q. Lu and G. Q. Lu, *J. Phys. Chem. B*, 2006, **110**, 16923.

7 (*a*) A. D. Becke, *Phys. Rev. A: At., Mol., Opt. Phys.*, 1988, **38**, 3098; (*b*) C. Lee, W. Yang and R. G. Parr, *Phys. Rev. B*, 1988, **37**, 785; (*c*) S. H. Vosko, L. Wilk and M. Nussair, *Can. J. Phys.*, 1980, **58**, 1200; (*d*) A. D. Becke, *J. Chem. Phys.*, 1993, **98**, 5648.

8 (*a*) G. Kresse and J. Furthmüller, *Comput. Mater. Sci.*, 1996, **6**, 15; (*b*) G. Kresse and J. Furthmüller, *Phys. Rev. B: Condens. Matter*, 1996, **54**, 11169; (*c*) G. Kresse and D. Joubert, *Phys. Rev. B: Condens. Matter Mater. Phys.*, 1999, **59**, 1758; (*d*) VASP the guide, http://cms.mpi.univie.ac.at/vasp/.

9 M. Gajdoš, K. Hummer, G. Kresse, J. Furthmüller and F. Bechstedt, *Phys. Rev. B: Condens. Matter Mater. Phys.*, 2006, **73**, 045112.

10 MedeA is commercialized by Materials Design Inc. http://www.materialsdesign.com.

11 L. M. Schabbach, F. Bondioli and M. C. Fredel, *J. Eur. Ceram. Soc.*, 2011, **31**, 659.

12 S. Zhi, *Optical electronics [M]*, Beijing, Science Press, OHM, 2001.

13 G. L. Chai, C. S. Lin, J. Y. Wang, M. Y. Zhang, J. Wei and W. D. Cheng, *J. Phys. Chem. C*, 2011, **115**, 2907.

14 A. G. Marinopoulos, L. Reining, A. Rubio and N. Vast, *Phys. Rev. Lett.*, 2003, **91**, 046402.

15 B. D. Cullity, *Elements of X-ray diffraction*, Addison-Wesley, Reading, MA, 1978.

16 G. Airey, *Constr. Build. Mater.*, 2002, **16**, 473.

17 (*a*) X. H. Lu and U. Isacsson, *Fuel*, 1998, **77**, 961; (*b*) I. Gawel and K. Baqinska, *Pet. Sci. Technol.*, 2004, **22**, 1261.

18 X. H. Lu and U. Isacsson, *Constr. Build. Mater.*, 2002, **16**, 15.

19 (*a*) M. N. Siddiqui and M. F. Ali, *Fuel*, 1999, **78**, 1005; (*b*) J. Y. Yu, P. C. Feng, H. L. Zhang and S. P. Wu, *Constr. Build. Mater.*, 2009, **23**, 2636.

 This journal is © the Owner Societies 2013